



BUREAU OF ECONOMIC GEOLOGY
THE UNIVERSITY OF TEXAS AT AUSTIN

*University Station, Box X • Austin, Texas 78713-8924 • (512) 471-1534 • FAX (512) 471-0140
10100 Burnet Road, Bldg. 130 • Austin, Texas 78758-4497*

Airborne Lidar survey of Frio River, Texas

**Project Report
-Final-**

RECEIVED

NOV 16 2018

TWDB CONTRACTS

Kutalmis Saylam, John R. Hupp, John R. Andrews and Aaron R. Averett

Contract Texas Water Development Board
Contract No. 1800012220

Near Surface Observatory,
Bureau of Economic Geology,
John A. and Katherine G. Jackson School of Geosciences,
The University of Texas at Austin



BUREAU OF ECONOMIC GEOLOGY
THE UNIVERSITY OF TEXAS AT AUSTIN

*University Station, Box X • Austin, Texas 78713-8924 • (512) 471-1534 • FAX (512) 471-0140
10100 Burnet Road, Bldg. 130 • Austin, Texas 78758-4497*

Airborne Lidar survey of Frio River, Texas

Project Report -Final-

Kutalmis Saylam, John R. Hupp, John R. Andrews and Aaron R. Averett

Contract Texas Water Development Board
Contract No. 1800012220

Near Surface Observatory,
Bureau of Economic Geology,
John A. and Katherine G. Jackson School of Geosciences,
The University of Texas at Austin

Table of Contents

1) Foreword.....	3
2) Materials and methods.....	5
a) Study area	5
b) Ground control.....	9
c) Lidar system calibration	9
d) Airborne missions	12
e) Lidar data acquisition.....	13
f) Aerial imagery	13
g) Sonar data acquisition	14
h) Water surface and bottom confirmation.....	16
i) Water clarity measurements	16
3) Findings and discussion.....	18
a) Water-bottom confirmation	18
b) Water-surface confirmation	19
c) Turbidity measurements.....	20
d) Sonar measurements.....	21
e) Lidar bathymetry and topography	23
4) Conclusion.....	26
References	27
Appendix A.....	30

1) Foreword

This project report acknowledges the efforts to acquire, process and analyze airborne Lidar bathymetry and aerial imagery of Frio River for research purposes. Texas Water Development Board (TWDB) funded the project, Texas Department of Transportation (TxDOT) carried out the airborne flight services, and Bureau of Economic Geology (BEG) at the University of Texas at Austin (UT Austin) researchers conducted the study in 2018. The end products - bathymetric and land surface elevation models - will be suitable for aquatic habitat modeling, bathymetry, hydrography, and other environmental studies.

Airborne Lidar Bathymetry (ALB) is a scientific technology for characterizing the depths of water columns in relatively shallow, clear waters from an airborne platform using a scanning and pulsed light beam. BEG owns and operates an ALB system, Leica AHAB “Chiroptera” (Fig. 1) and have access to survey aircrafts with varying mission capability (Fig. 2). The system uses a near-infrared (NIR) wavelength (1 nm) for topographic and a green wavelength (0.5 nm) for the bathymetric data collection. The effective range is 400 to 500 m for bathymetric scanner, which acquires data with a continuous waveform signal. The topographic scanner enables surveys at 1,500 m above ground level and can record pulses up to 400 kHz at lower altitudes. Both scanners direct the light beam with a fixed incident angle of 14° at fore and aft, and 20° to each side, creating an elliptical pattern on the surface. The Palmer scanner has advantageous over an oscillating pattern with its capability to map the sloped surfaces, and underneath the canopies at certain scan angles. Additionally, ALB systems integrate cameras on board with either natural or spectral imaging capabilities for acquiring high resolution imagery simultaneously with Lidar data acquisition.

Bathymetry is the foundation of the science of hydrography which measures the physical features of a water body. Bathymetric surveys allow us to measure the depth of distinctive water bodies and understand the hydrologic and geologic properties such as contour modeling, flood inundation, leakage, scour and stabilization, and benthic zone formations. Certain practices are required to undertake such surveys; generally, the type of water body, water transparency, depth, accuracy requirements, and the potential

cost determines the methodology. For shallow water surveys, ALB have proved to be a versatile, cost-effective, and detailed method compared to other remote sensing technologies such as sonar and satellite imaging (Ebrite et al., 2001; Guenther et al., 2002). A number of river surveys have been conducted using ALB technology in the recent years (Hilldale and Raff, 2008; Kinzel et al., 2013; Legleiter, 2012; Mandlbürger et al., 2013; Pan et al., 2015; Saylam, 2016) and results proved it as a viable and an accurate method for geologic mapping and habitat monitoring. However, river projects can be complicated as there are various limiting aspects, especially with surveying the water near the riparian areas (Mandlbürger et al., 2013; McKean et al., 2014). In general, overhanging vegetation limit the Lidar beams and create a shadow effect underneath in the point cloud data. The scanning pattern of Chiroptera is advantageous for river surveys with overhanging riparian vegetation since it is possible to scan underneath the canopies at certain angles. In this project, to minimize shadow effects, we approached pool locations from different angles, and conducted dual-beam echo sounder (sonar) surveys in conjunction with airborne data acquisition.

BEG has been involved in airborne Lidar surveys (ALS) since 2000 (Paine et al., 2005, 2004) and has completed hundreds of ALB survey hours at diverse locations and conditions, applying specific know-how and quality management methods (Saylam et al., 2018). Because this study had specific objectives, and challenging conditions, the foremost objective was to demonstrate the applicability of ALB technology to map the water bottom of a densely vegetated river riparian zone. The final product desired was a bare earth model. Furthermore, we correlated ALB results with other supplemental surveys (e.g. sonar, water transparency, GPS) for accuracy and knowledge base.



Figure 1: Leica AHAB Chiroptera.



Figure 2: Chiroptera was installed in a Texas Department of Transportation (TxDOT) owned and operated Cessna 206.

2) Materials and methods

a) Study area

Frio River, begins in northeast Real County and flows in southeasterly direction for about 400 km, traversing Uvalde, Medina, Frio, La Salle, McMullen and Live Oak counties of Texas. Figure 3 presents the survey location at north of Leakey, Texas ($29^{\circ}45'13''$ N, $99^{\circ}45'30''$ W) where northern sections of the river winds through Frio Canyon. The stream passes through limestone formed canyons lined with a variety of trees. Upper sections of the river - north of US-90 highway - are very scenic and hanging trees provide a shaded setting for recreational activities while maintaining an ecologically diverse environment. The aquatic and riparian habitats of the Frio River considered to support an exceptionally diverse assemblage of invertebrates, fish, birds, aquatic weeds and plants of Edwards plateau (Figs. 4 & 5) (Norris et al., 2005).

There are numerous springs along the river and these provide valuable discharge and recharge along the outcrop portion of the Edwards Aquifer. The river ultimately empties into the Nueces River, contributing freshwater inflow to Nueces and Corpus Christie bays on the Texas Gulf coast. However, in 2018, USGS

gage¹ in pool 15 (Fig. 6) (29° 29' 19.04 N, 99° 42' 16.94 W) indicated less discharge and height levels compared to 2017 for the month of April. Figures 8 and 9 illustrate monthly discharge and height levels where median discharge rate was 51 ft³/sec (1.44 m³/sec) and gage height is 3.67 ft. (1.12 m). We identified 15 pools that have substantial water storage throughout the survey area. These locations are illustrated in Figure 3. We had access to some of these pools with a kayak, and were able to complete supplementary surveys with sonar and GPS (Fig. 7).

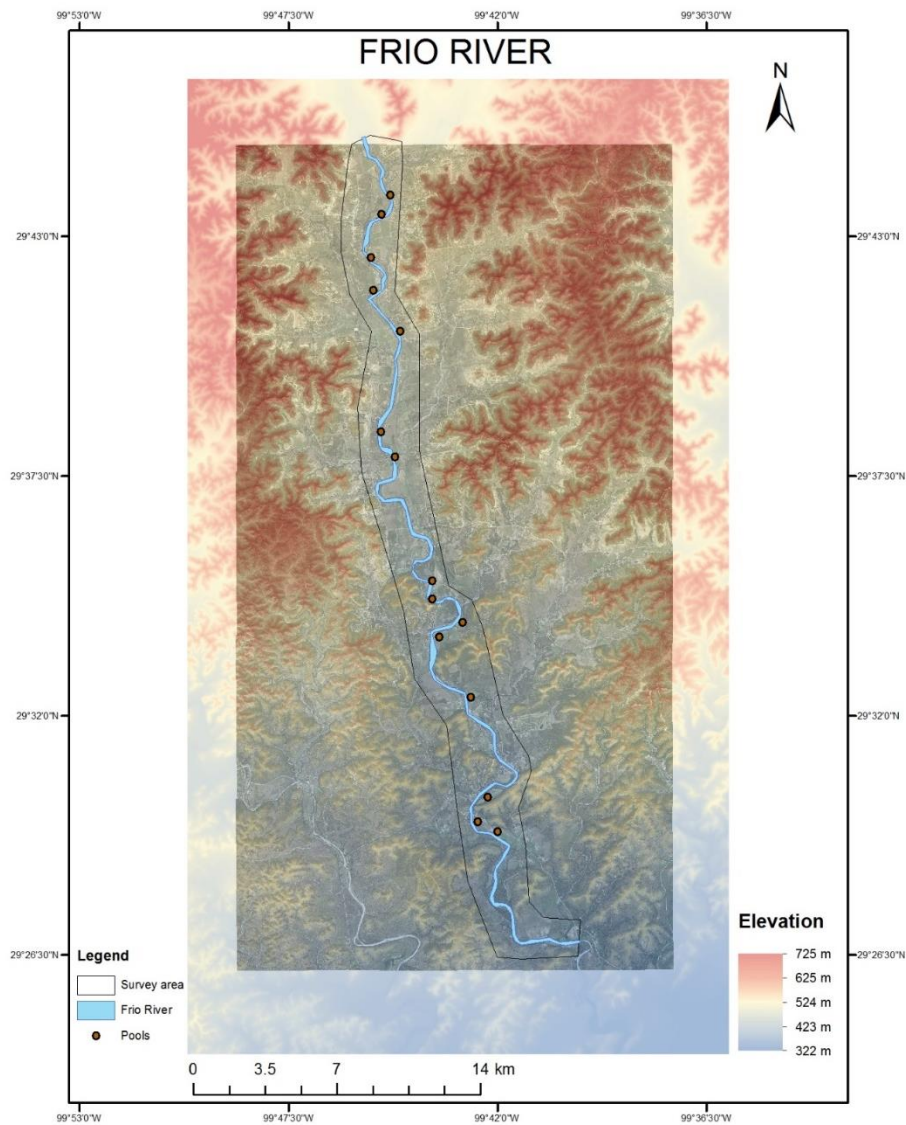


Figure 3: Frio River study area. Pools are numbered in sequence from 1 to 15, north to south.

¹ National Water Information System, USGS 081950000 Frio River at Concan, TX.



Figure 4: Frio River and its scenic environment, surrounded by overhanging trees at riparian zone.



Figure 5: Diverse submerged assemblage, which creates challenges for Lidar and sonar measurements.



Figure 6: USGS gage.

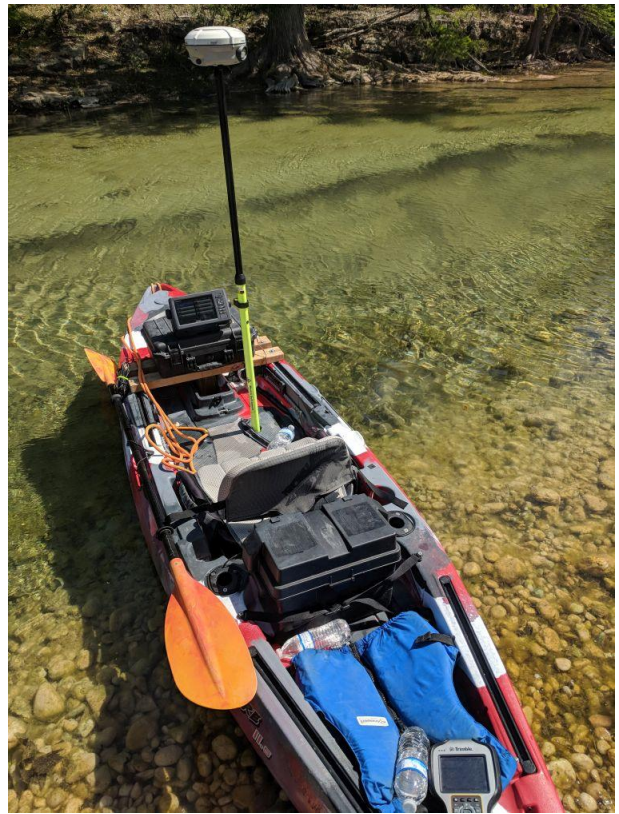


Figure 7: Sonar and survey kayak.

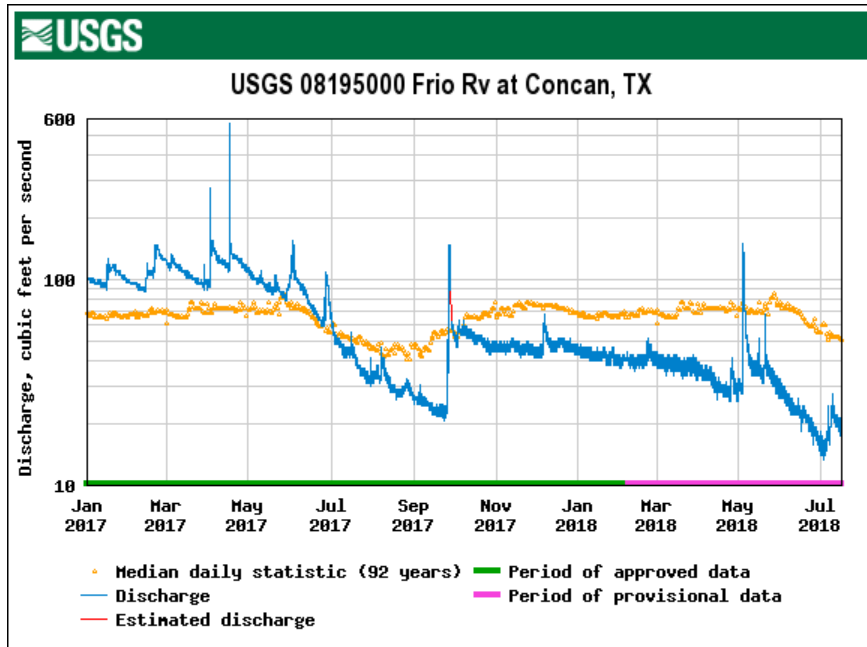


Figure 8: 2017 and 2018 discharge rates as measured by USGS gage at Concan, Texas location.

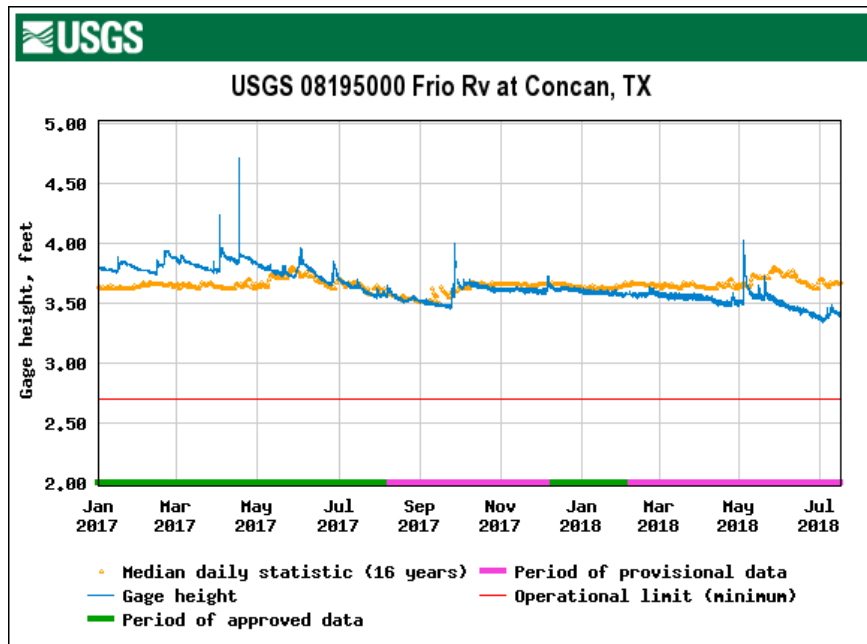


Figure 9: 2017 and 2018 water-column levels as measured by USGS gage at Concan, Texas location.

b) Ground control

Acquiring precise geodetic level ground control data with GNSS receivers is critical for producing accurate airborne Lidar datasets. Continuously Operating Reference System (CORS) is a network operated by local agencies, and overseen by U.S. National Geodetic Survey. We had online access to TXUV (Uvalde) and TXLE (Leakey) which are maintained by TxDOT. Both stations were strategically located for airborne survey purposes, and they sampled data in 1-second increment. BEG researchers also setup a reference station for backup purposes at Whiskey Mountain, TX location but this was not used due to highly accurate data availability from CORS stations. Table 1 illustrates the locational and mean accuracy findings, and Appendix A presents measurement findings of both stations in all directions (X, Y and Z) in 2018.

Table 1: CORS stations information and accuracy in 2018.

Reference station	Latitude	Longitude	Ellipsoidal height (H, m)	Mean accuracy (N, cm)	Mean accuracy (E, cm)	Mean accuracy (Z, cm)
TXUV	29°12' 01.86729	99°49' 37.57853	262.570	0.07	0.04	0.84
TXLE	29°44' 21.58283	99°45' 40.5039	478.402	1.57	-0.01	-0.41

c) Lidar system calibration

A total of 175 ground control points were acquired over the taxiway surface at Del Rio, TX airport (DRT) using a geodetic level GPS receiver (Trimble R8 GNSS). These precise control points were used to understand and adjust the slant range correction (vertical biases) of Lidar returns. Because topographic and bathymetric scanners function independently, it was important to understand and correct the common offset errors of both scanners and minimize them in order to have a seamless data set. Figure 10 illustrates the control points acquired in March 20th, 2018.

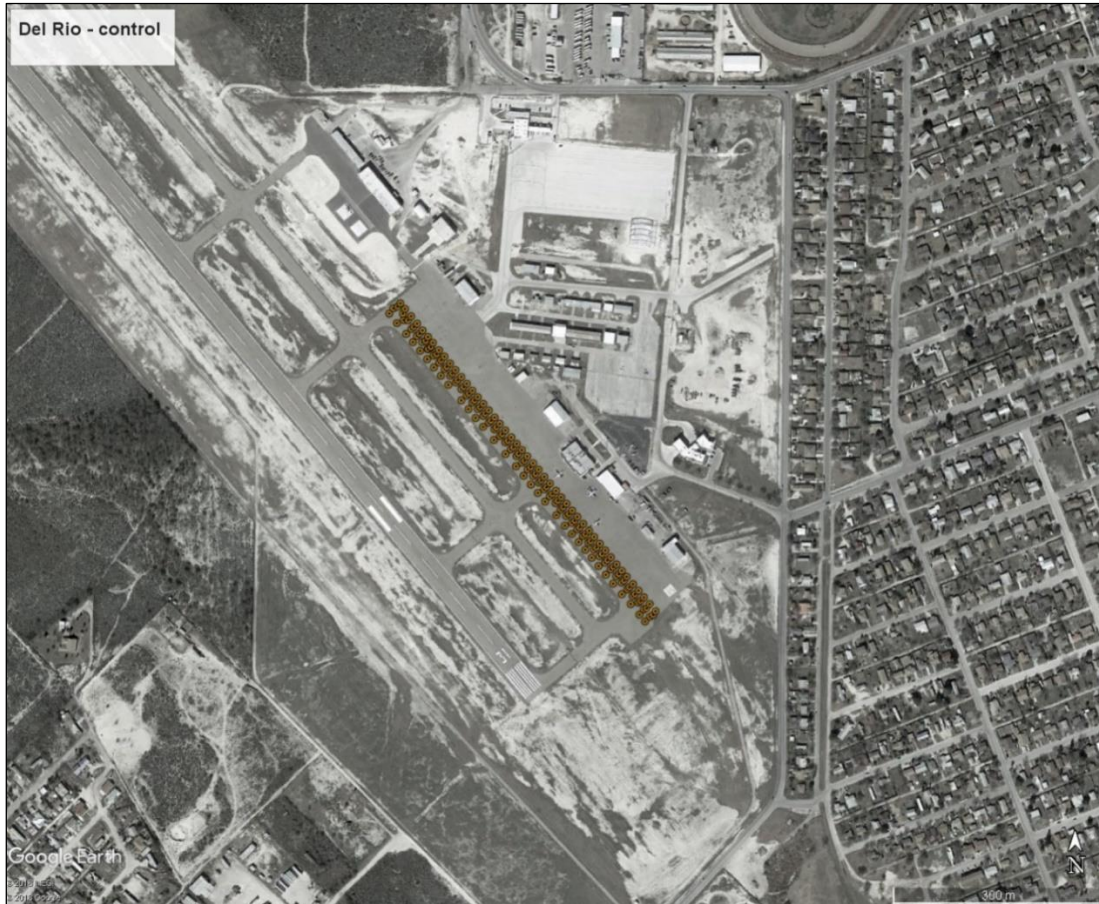


Figure 10: Control points at Del Rio International Airport taxiway.

We compared ground control points to Lidar returns using the least squares statistical approach. We calculated the fit with polynomial regression, and computed the R^2 measure value, which is the percentage of the response variable variation, representing the closeness of data. Additionally, the root-mean-square-error (RMSE) is a frequently used statistical measure of the differences between values predicted by a model and the values observed.

Table 2 presents the findings and Figures 11 and 12 illustrate the fit between both scanners to the ground control points. For both scanners, median bias was less than 2 cm, and standard deviation was calculated at 3 cm. Elevation heights calculated in this practice are ellipsoidal, native and true to GPS and Lidar data acquisition. We converted the ellipsoidal elevations to orthometric height (real world elevations) using the GEOID2012B Geoid model to produce the end products.

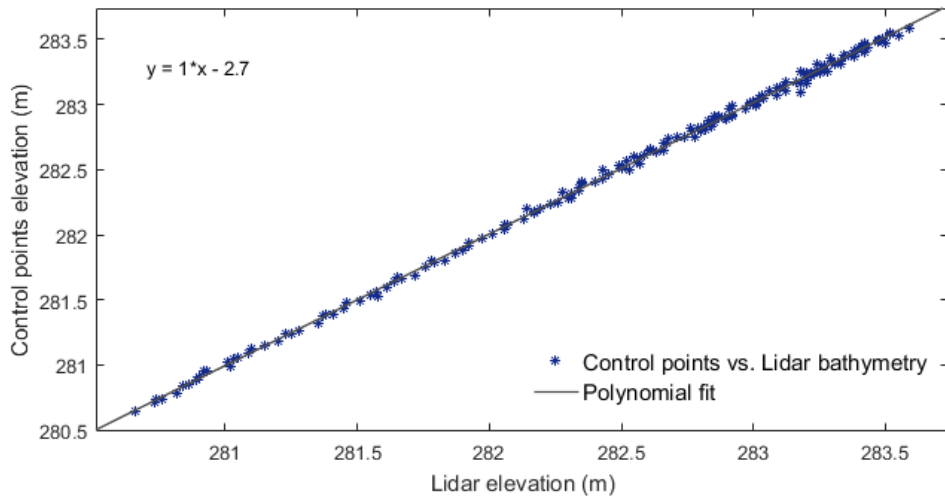


Figure 11: Chiroptera bathymetric scanner slant range adjustment results ($R^2=0.999$).

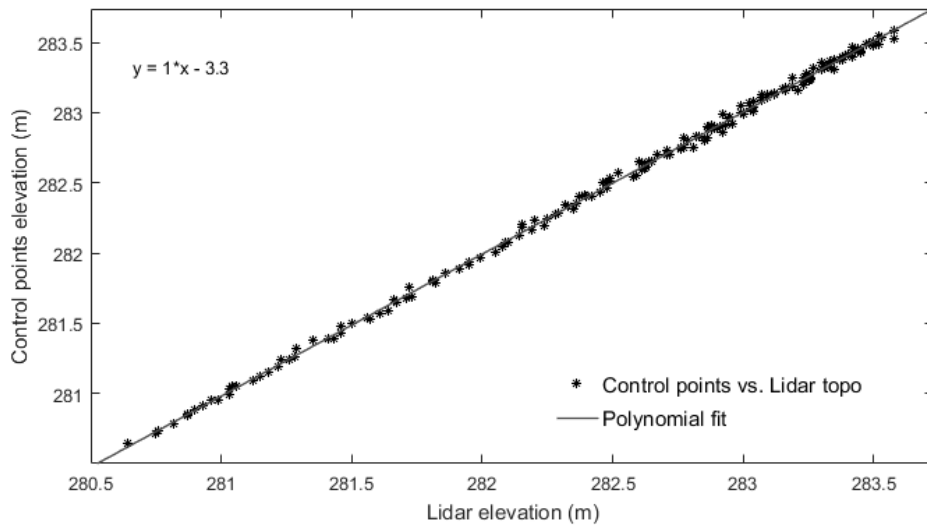


Figure 12: Chiroptera topographic scanner slant range adjustment results ($R^2=0.998$).

Table 2: Chiroptera system calibration, vertical bias adjustment results

Scanner	Number of samples	Range (m)	Median (m)	SD (m)	RMSE (m)	R-squared
NIR	182	0.13	0.004	0.03	0.026	0.998
Green-wavelength	182	0.16	0.016	0.03	0.026	0.999

d) Airborne missions

The contractual requirement indicated flying at 800 m and 400 m for separate purposes (topo and bathymetry). Because of variable weather conditions at the location, we eliminated higher altitude mission and completed entire survey at 400-450 m, which is the optimum altitude for bathymetric Lidar data collection. However, this increased the number of flight lines, and the duration to complete the acquisition stage. A total of 101 individual flight lines were flown with TxDOT aircraft, and detailed mission information is illustrated in Table 3. Uvalde Garner Field airport was used as the base airport for all missions. Total airborne survey time was 15:06 h, excluding mobilization time from and back to Austin. Airborne missions were completed at an average ground speed of 120 knots/hour. Flight lines were separated by approximately 160-180 m from each other to achieve a minimum of 40% overlapping. Swath on the ground was measured to have a minimum of 250 m width as this was a critical consideration given that the ground altitude of the survey location highly varied, and any lesser amount of side overlapping would create gaps between the strips. However, due to abrupt elevation changes in the southern sections of the survey location, multi-pulse errors were experienced with some flight lines during topographic data acquisition. This is a typical occurrence when Lidar repetition rate does not support the range (distance) as the beam is transmitted and received, resulting in weak amplitude. For instance, 300 kHz of repetition rate is excessively ‘fast’ at 500 m range for receiving returning pulses where 220 kHz would suffice. These lines were repeated with additional missions on the 04/23 with slightly lower repetition rate (240 versus 260 KHz).

Table 3: Airborne mission information

Date	Duration (h)	Altitude (m, GPS)	Flight lines
04/10/2018	3:13	3,000	1-25, 83-88
04/10/2018	1:22	2,900	26-34
04/10/2018	3:04	2,900	35-39, 47-55, 40-46, 98-99
04/16/2018	3:02	2,900	74-82, 89-97, 100-101
04/23/2018 - repeat	2:23	2,800	1-22, 39-40
04/23/2018 - repeat	2:02	2,800	23-38

e) Lidar data acquisition

Topographical and bathymetric data were acquired simultaneously on all missions. A total of 5,042,555,791 discrete returns were output for topographical data sets, and 10,943,735 for bathymetric data sets. Bathymetric returns are a product of waveform information, and the most distinctive two peaks represent water surface and bottom. For ease of data processing, we divided the survey area into 18 blocks, in 2 km partitions, and named them sequentially from north to south. As the project deliverable, we will truncate data further to 1x1 km for easier visualization and analysis.

Because we acquired data at lower altitudes, higher repetition rate (260 kHz) was used for topographical data collection. This enabled much denser data collection on the ground. We averaged **30 points/m²** at flat ground areas, instead of 4 points/m² per contract. Bathymetric data set averaged 1.65 points/m² due to its fixed repetition rate at 35 kHz.

Point cloud Lidar data is output in Las v1.2. There are 2 classes for bathymetric data; Class 0 and 7 which represent water surface and bottom respectively. Topographic data is Class 9, and vegetation is classified in three classes 13, 14 and 15. However, we did not complete a rigorous vegetation separation with point cloud data, but removed all evident vegetation to build the bare earth model.

f) Aerial imagery

Chiroptera has an enclosed medium format Hasselblad H4D-50 camera with a 50.3mm focal length. A total of 2,731 high-resolution, natural color (RGB) images were acquired in conjunction with Lidar data. The resolution of these images average 5 to 6 cm/pixel and they are highly effective for distinguishing land and water characteristics. Each image becomes 147 MB in size when converted from a native Hasselblad '3fr' format to a more user-friendly 'tiff' format. For orthophoto building purposes, we scaled the resolution to 25 cm, enabling less distortion and better color balancing between the images.



Figure 13: Example of an aerial image collected over the Frio River.

g) Sonar data acquisition

In shallow and calm waters, the surface and bottom position peaks indicated with bathymetric waveform data may become mixed and can be difficult to distinguish (Allouis et al., 2010). In addition, river crossings, overhanging trees, and aquatic habitat may block Lidar beams. In such adverse conditions, sonar measurements may provide depth and confirm bathymetric Lidar returns, providing additional means to understand the depth of the water column. On the Frio River, we had access to 7 of 15 pools for sonar surveys, and measurements were conducted especially in the sections where trees blocked the river. A custom-built kayak with a trolling engine was an ideal platform because of its mobility and capability to maneuver in tight and shallow areas of the river (Figs. 14 and 15).

The sonar unit, Garmin 74dv, collects data up to 200 kHz with dual-beam technology and the effective depth range is rated at 700 m with 77 kHz scanning speed, in fresh water bodies. It also samples

positional data at a rate of 5 Hz with a built-in GPS interface. In the lab environment, we tested the unit to produce standard deviation accuracy of 2.7 cm at a depth of 11.8 m depth. Because the Frio River is shallow and mostly calm, we did not consider rotational angle adjustment for roll, pitch and attitude information. However, such computations should be considered for deeper and choppier water body surveys. Throughout the river, we measured 0.36 m as the shallowest, and 4.67 m as the deepest water column (Fig. 16).



Figure 14: Kayak with sonar equipment.



Figure 15: Calm and shallow waters of the Frio River.

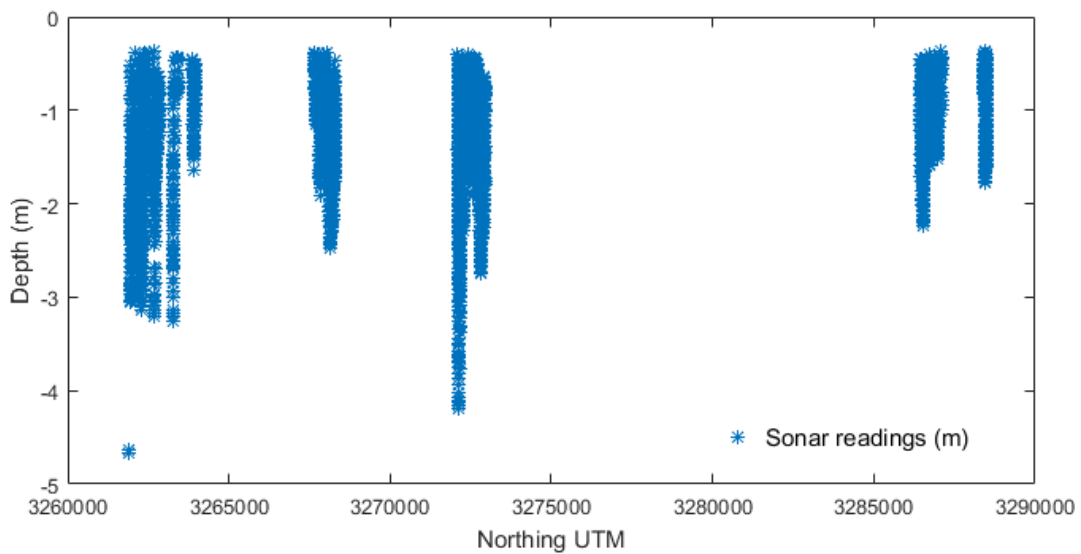


Figure 16: Sonar measurements at selected pools in the Frio River survey.

h) Water surface and bottom confirmation

We measured water surface and bottom at designated locations throughout the river using a geodetic grade GPS receiver (Trimble R8) with a 2 m pole. In practice, it is difficult to steadily measure water surface, especially from a boat, so minor variations may exist and should be regarded as acceptable. For bottom measurements, we used rock surfaces mostly to prevent sinking.

Surface and bottom measurements are generally required to confirm the accuracy of ALB and should be conducted simultaneously with airborne missions. Ideally, the measuring GPS pole should have a flat end to prevent sinking in the water column or in the bottom. One can simply survey the depth by using a simple measuring device (e.g. marked rod), but such measurements would require positional information and may not be ideal at deeper and faster flowing conditions. Our findings indicated Lidar returns to have tight correlation with water-bottom measurements, and minor variation with surface realization.

i) Water clarity measurements

A challenging task for an ALB survey is understanding the water conditions (transparency) and its effects on Lidar bathymetry. Because organic and other suspended material in the water-column scatter and attenuate the light beam energy quickly, it is significant to understand the conditions in quantitative terms. There are no specified requirements for ALB surveys, but rather suggested values indicating transparency. The Secchi depth, the maximum depth at which a white and black circular disk of 30 cm diameter, (Fig. 17) can be seen when progressively lowered into a water body, is not a definite predictor of ALB survey performance, but rather a guide to calculating the diffuse attenuation coefficient (Preisendorfer, 1986). There are different style Secchi disks, for marine and fresh waters, and these differ by their size and design. Chiroptera is rated at 1.5 times the Secchi depth by the manufacturer at ideal water conditions when benthic zone reflectance conditions are greater than 15%. Several articles provide information and discuss the effects of diffuse attenuation on ALB performance (Banic and Sizgoric, 1986; Churnside et al., 1998; Lee, 2005).

Turbidity is an expression of the optical property that causes light to be scattered and absorbed rather than transmitted in straight lines through the sample (Jethra, 1993; Suk et al., 1998) and is expressed in nephelometric turbidity units (NTU) in the United States. Turbidity causes light beams to scatter in the water column where particle size, shape, and composition may all affect its amplitude (Baker and Lavelle, 1984; Bhargava and Mariam, 1991). Turbidity was measured with a portable field turbidimeter that complies with Environmental Protection Agency (EPA) method 180.11 (O'Dell, 1993). The Hach 2100Q measures turbidity between 0 and 1,000 nephelometric turbidity units (NTU), with a resolution of 0.01 NTU (Fig. 18).

In 2014, Chiroptera's manufacturing company (AHAB) developed a turbid water enhancement algorithm that omits some of the weaker backscatter noise created by low or moderate levels of turbidity and selects the most distinctive peak as the water-bottom reflectance. In previous projects, we observed respectable gains -up to 41%- in turbid and shallow waters (Saylam et al., 2018). Additionally, the algorithm also demonstrated performance benefits in deeper and cleaner waters where average turbidity levels were less than 1 NTU (Saylam et al., 2017).

For this project, we conducted turbidity and Secchi disk measurements throughout the river at selected locations. Because the water was transparent and water-column depth did not exceed visual limits, Secchi disk measurements were not necessary. We observed Secchi disk at the water bottom clearly at all locations. Turbidity levels were low, and were not considered as a challenging medium for overall ALB surveys.



Figure 17: Secchi disk.



Figure 18: Field turbidimeter.

3) Findings and discussion

Foremost, we analyzed the robustness of bathymetric Lidar measurements using GPS (Trimble Net R9 GNSS) at certain pools. Because of tall trees and high cliffs, GPS signals were partially blocked at some locations, especially at pool 9 by Garner State Park. Post processing of GPS revealed typical standard deviation values for vertical measurements (Table 4).

Table 4: GPS post processing quality-control findings (vertical adjustment)

Measurement	Number of samples	Data range (m)	Median (m)	SD (m)
Water surface	28	0.11	0.04	0.02
Water bottom	40	0.08	0.05	0.01

a) Water-bottom confirmation

We collected a total of 40 water bottom measurements (control points) using a Trimble R8 GNSS receiver and correlated these to bathymetric Lidar returns. We used the Delaunay algorithm to build triangulated irregular network (TIN) patches of Lidar returns that register within 2 m of a control point, sloping less than 30 degrees, and evaluated findings. Results indicated a good correlation and a normal distribution (Fig. 19), median was -0.022 m and standard error at 0.015 m (Lidar returns versus control points). Table 5 illustrates findings of each individual pool where measurements were conducted. Overall, $R^2 = 0.929$ indicated a robust correlation.

Table 5: Comparison of water-bottom measurements to Lidar-derived elevations

Pool	Number of samples	Median (m)	Average depth (m)	RMSE (m)	R-squared
2	14	-0.004	1.10	0.066	0.958
3	11	-0.033	1.07	0.063	0.967
9	8	-0.013	0.73	0.055	0.915
12	7	-0.024	1.08	0.125	0.878

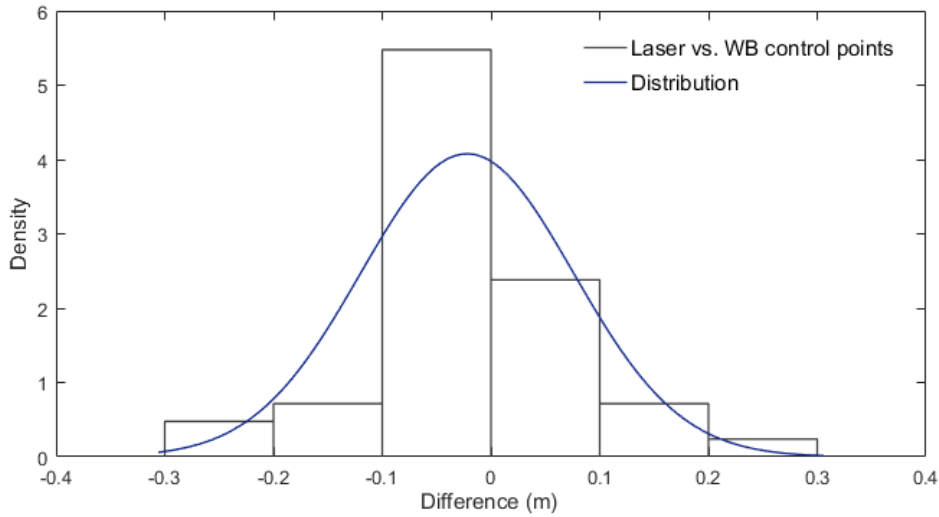


Figure 19: Distribution of water-bottom control points to Lidar returns.

b) Water-surface confirmation

We measured water surface at 28 selected locations. Median difference of all measurements was calculated at -0.056m (Lidar returns versus control points). Of all pools, averaged standard deviation was 0.036 m (Table 6). The discrepancy may have been caused by less than ideal GPS signal reception at certain locations, especially in pools 2 and 9. Surrounding tall trees and high cliffs blocked some measurement locations, and these may have caused higher overall PDOP values, leading to poorer accuracy. Nevertheless, results are satisfactory and contribute to overall confidence of Lidar findings.

Table 6: Water-surface measurement comparison to Lidar-derived surface realization

Pool	Number of samples	Range (m)	Median (m)	SD (m)	RMSE (m)
2	8	0.06	-0.10	0.02	0.02
8	6	0.12	-0.04	0.02	0.02
9	2	0.16	-0.10	0.04	N/A
12	4	0.07	-0.01	0.04	0.05
15	8	0.15	-0.03	0.06	0.03

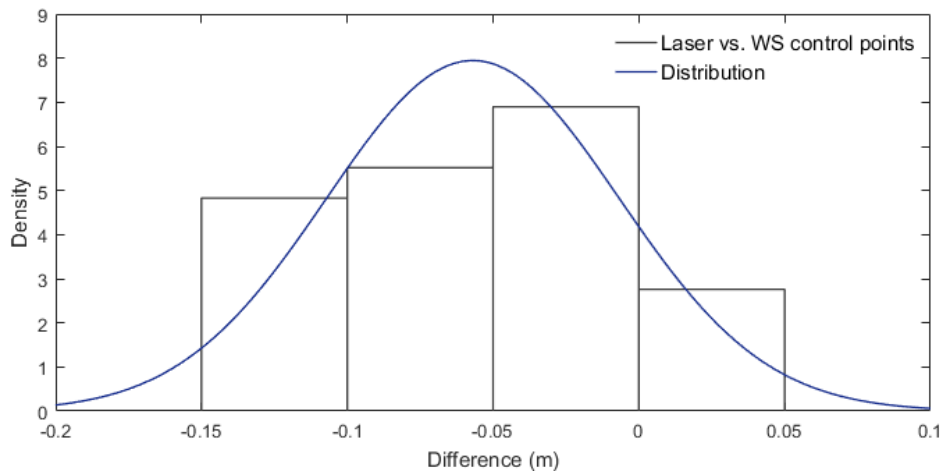


Figure 20: Distribution of water-surface measurements to Lidar surface realization.

c) Turbidity measurements

We sampled water conditions at selected locations throughout the river and found turbidity levels at ideal levels for ALB surveys (Fig. 21). In each sampling location, we conducted 3 readings, and these were averaged. Standard deviation was calculated at less than 0.15 NTU for all measurements (Table 7). Results indicated the overall turbidity level less than 1 NTU and water-column depth shallower than 3.2 m, which is ideal for bathymetric Lidar surveys (Saylam et al., 2018). Under such conditions, it is expected that Lidar beams would penetrate to the bottom and reflect back to the receiver with sufficient amplitude.

Table 7: Turbidity and depth measurements at selected locations in the Frio River

Pool	Location (N, W)	Median NTU	SD	Depth (m)
2	29° 43' 28.07, 99° 44' 56.75	0.42	0.02	1.40
3	29° 42' 31.17, 99° 45' 25.12	0.66	0.15	1.38
3	29° 42' 23.84, 99° 45' 19.67	0.43	0.02	2.09
8	29° 32' 31.85, 99° 42' 52.83	0.44	0.03	2.10
8	29° 32' 19.93, 99° 42' 48.67	0.48	0.05	1.11
9	29° 29' 19.12, 99° 42' 22.74	0.59	0.03	3.20
9	29° 29' 17.62, 99° 42' 9.90	0.57	0.12	1.90
10	29° 29' 8.16, 99° 41' 55.54	0.76	0.04	1.73
10	29° 34' 59.43, 99° 43' 45.43	0.55	0.04	1.35

15	29° 34' 46.16, 99° 43' 51.24	0.46	0.06	2.06
15	29° 34' 37.06, 99° 43' 42.29	0.58	0.16	2.63
15	29° 34' 36.90, 99° 43' 40.50	0.39	0.03	1.78



Figure 21: Turbidity measurement location at pool 15, depth 2.06 m.

d) Sonar measurements

Approximately 15,000 sonar measurements were acquired in conjunction with airborne missions. It was critical to schedule airborne and sonar surveys at similar schedules for depth consistency.

We have correlated a total of 10,600 sonar measurements to Lidar returns at respective pools. Again, a TIN patch was created with all bathymetric Lidar returns at a plane and 2 m distance to a sonar measurement, not exceeding 30-degree slope.

Findings indicated an average median value of 9 cm and standard deviation of 30 cm (Table 8). Results are typical for shallow and calm waters with varying aquatic assemblage and hanging trees that prevent the Lidar signals reaching the water bottom. Especially in pool 9, sonar measurements were completed in shadow areas where Lidar signals were mostly blocked, resulting in poor correlation probability at depths

of 2 m and greater where sonar penetrated deeper (Fig. 22). Pool 8 findings indicated the lowest median difference, and a good probability that Lidar and sonar readings mostly matched each other (Fig. 23).

Table 8: Sonar readings correlation results to Lidar-derived patch elevations at water bottom

Pool	Samples	Median (m)	SD (m)	RMSE (m)	R-squared
3	1843	0.14	0.2	0.2	0.812
8	1584	0.06	0.21	0.2	0.832
9	1840	0.06	0.58	0.48	0.382
12	2156	0.06	0.24	0.23	0.681
13	176	0.07	0.2	0.2	0.631
14	522	0.11	0.35	0.34	0.912
15	2479	0.13	0.34	0.33	0.786

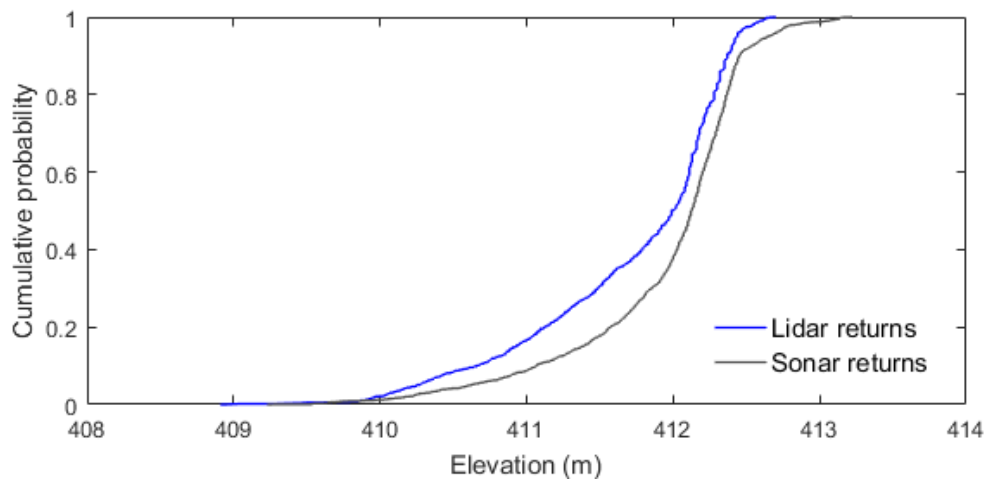


Figure 22: Pool 9, Lidar versus sonar returns

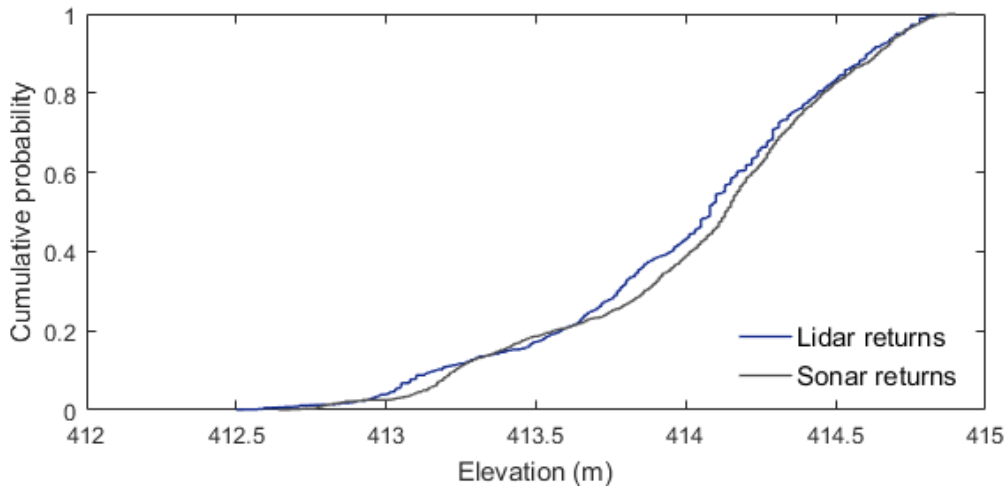


Figure 23: Pool 8, Lidar versus sonar returns

e) Lidar bathymetry and topography

At most locations throughout the river, bathymetric Lidar penetrated to the water-bottom. We generated statistics of selected pools, based on high and low points. Figure 24 and Table 9 present water surface and bottom findings. Figures 25 and 26 illustrate DEM representation of Garner State park with all features as collected, and all stripped off. Figure 27 represents LAS point cloud data, combination of topographical and bathymetric data, with water surface and bottom as a cross section.

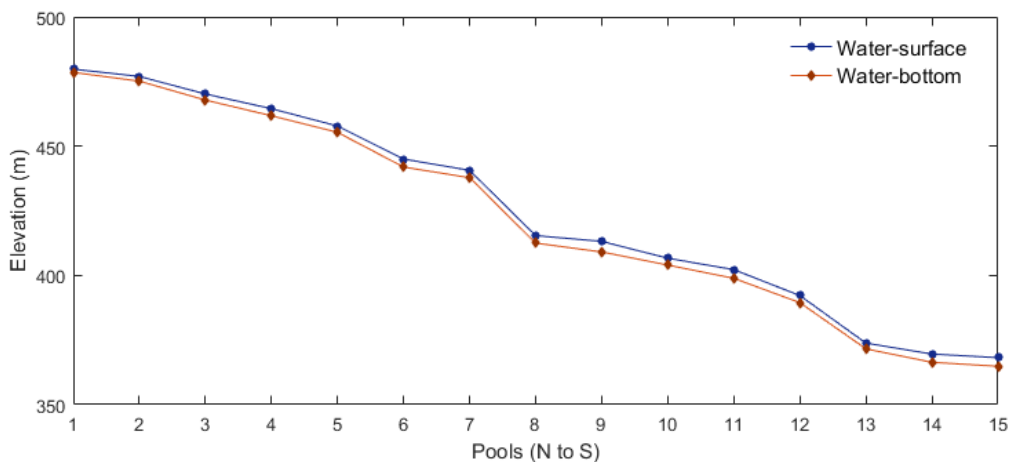
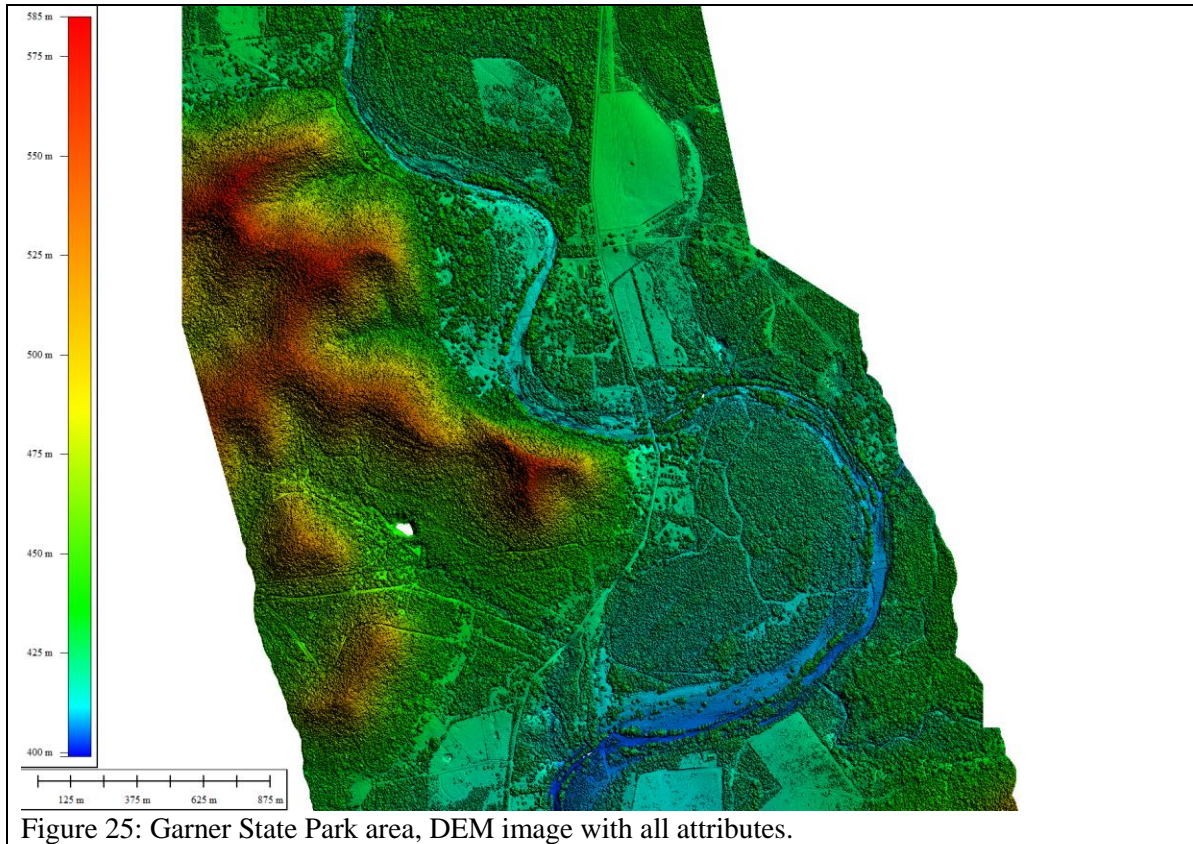
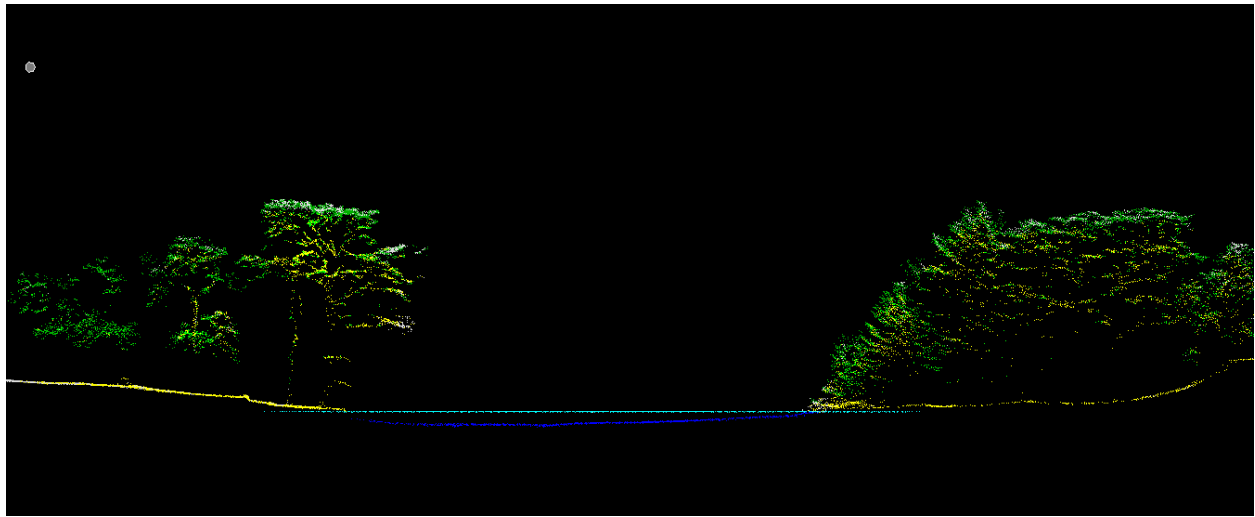
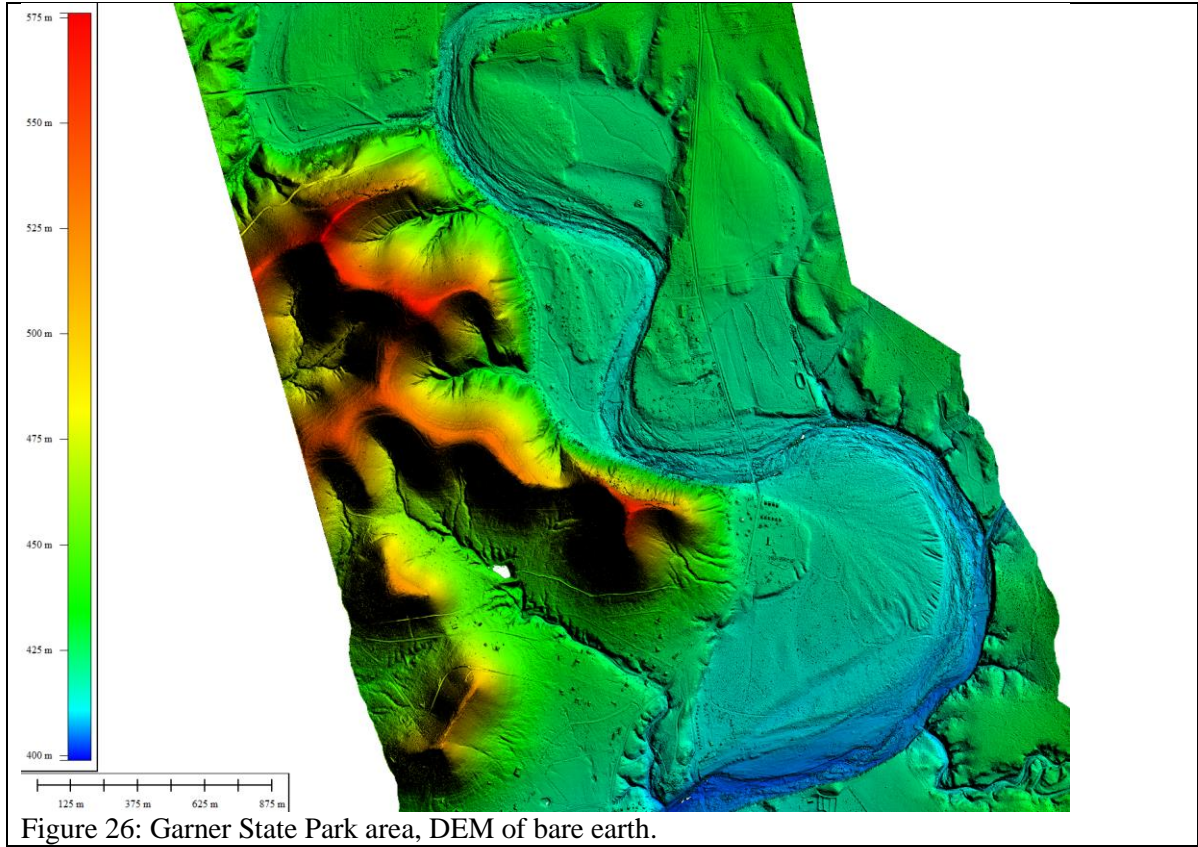


Figure 24: Lidar bathymetry at selected pools.

Table 9: Water surface, bottom and depth findings at selected pools

Pool	WS high (m)	WS low (m)	WS diff. (m)	WB low (m)	Max. depth (m)
1	479.78	479.53	0.25	478.52	1.01
2	476.96	476.91	0.05	475.13	1.83
3	470.17	470.04	0.13	467.81	2.36
4	464.48	464.31	0.17	461.75	2.73
5	457.77	457.66	0.11	455.33	2.44
6	445.01	444.74	0.27	441.91	3.1
7	440.63	440.26	0.37	437.78	2.85
8	415.39	415.18	0.21	412.5	2.89
9	413.16	413.13	0.03	409.05	4.11
10	406.64	406.43	0.21	404	2.64
11	402.22	401.85	0.37	398.87	3.35
12	392.2	391.93	0.27	389.45	2.75
13	373.81	373.51	0.3	371.59	2.22
14	369.59	369.45	0.14	366.37	3.22
15	368.17	367.92	0.25	364.85	3.32





4) Conclusion

This report summarizes the efforts to map the Frio River with airborne Lidar. We acquired bathymetric and topographic Lidar data, aerial imagery, and conducted supplemental surveys to assess the accuracy of the Lidar measurements. End products include point cloud LAS data and 1-m DEM representation of topographical and bathymetric areas as mapped.

Lidar revealed amazing levels of detail of the river geomorphology. Bare earth representation is an airborne Lidar strength, added to bathymetric representation of the river bottom. We believe, the end products of this study can be used for a variety of applications; geomorphological and geologic mapping, environmental assessment, floodplain mapping, forestry, and hydrography.

References

- Allouis, T., Bailly, J.-S., Pastol, Y., Le Roux, C., 2010. Comparison of Lidar waveform processing methods for very shallow water bathymetry using Raman, near-infrared and green signals. *Earth Surface Processes and Landforms* 35, 640–650. <https://doi.org/10.1002/esp.1959>
- Baker, E.T., Lavelle, J.W., 1984. The effect of particle size on the light attenuation coefficient of natural suspensions. *Journal of Geophysical Research* 89, 8197. <https://doi.org/10.1029/JC089iC05p08197>
- Banic, J., Sizgoric, S., 1986. Scanning Lidar bathymeter for water depth measurement, in: Cruickshank, J.M., Harney, R.C. (Eds.), pp. 187–195. <https://doi.org/10.1117/12.938673>
- Bhargava, D.S., Mariam, D.W., 1991. Light penetration depth, turbidity and reflectance related relationship and models. *ISPRS Journal of Photogrammetry and Remote Sensing* 46, 217–230. [https://doi.org/10.1016/0924-2716\(91\)90055-Z](https://doi.org/10.1016/0924-2716(91)90055-Z)
- Churnside, J.H., Tatarskii, V.V., Wilson, J.J., 1998. Oceanographic Lidar attenuation coefficients and signal fluctuations measured from a ship in the Southern California Bight. *Applied Optics* 37, 3105. <https://doi.org/10.1364/AO.37.003105>
- Ebrite, S., Pope, B., Lillycrop, W.J., 2001. A multi-agency solution for coastal surveys - SHOALS in the Pacific. *Marine Technol. Soc*, pp. 1204–1211. <https://doi.org/10.1109/OCEANS.2001.968284>
- Guenther, G.C., Lillycrop, W.J., Banic, R.J., 2002. Future advancements in airborne hydrography. *International Hydrographic Review*, New series 3, 67–90.
- Hilldale, R.C., Raff, D., 2008. Assessing the ability of airborne Lidar to map river bathymetry. *Earth Surface Processes and Landforms* 33, 773–783. <https://doi.org/10.1002/esp.1575>
- Jethra, R., 1993. Turbidity measurement. *ISA Transactions* 32, 397–405. [https://doi.org/10.1016/0019-0578\(93\)90075-8](https://doi.org/10.1016/0019-0578(93)90075-8)

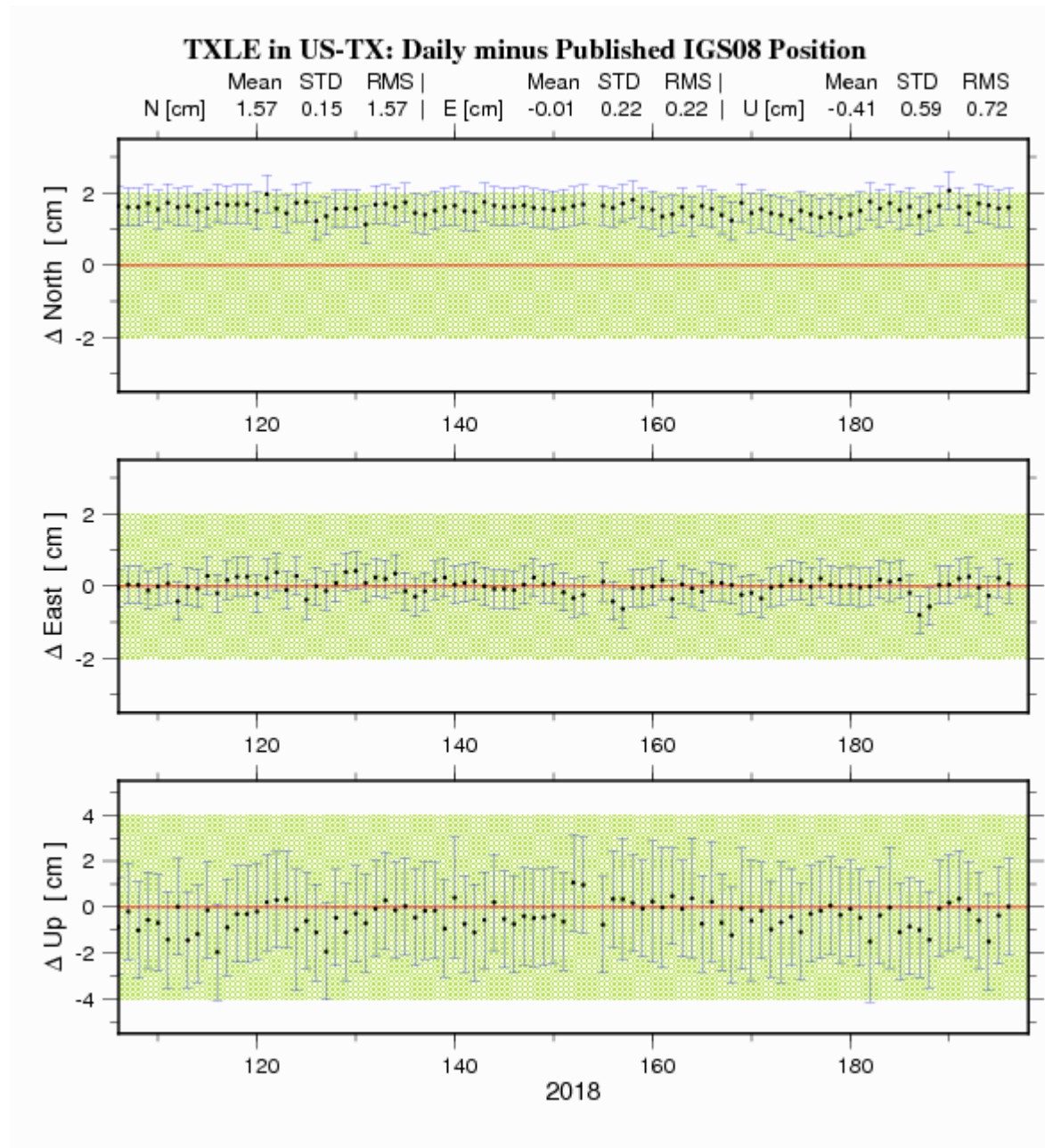
- Kinzel, P.J., Legleiter, C.J., Nelson, J.M., 2013. Mapping river bathymetry with a small footprint green Lidar: applications and challenges. *JAWRA Journal of the American Water Resources Association* 49, 183–204. <https://doi.org/10.1111/jawr.12008>
- Lee, Z.-P., 2005. Diffuse attenuation coefficient of downwelling irradiance: An evaluation of remote sensing methods. *Journal of Geophysical Research* 110, 1–9. <https://doi.org/10.1029/2004JC002573>
- Legleiter, C.J., 2012. Remote measurement of river morphology via fusion of Lidar topography and spectrally based bathymetry. *Earth Surface Processes and Landforms* 37, 499–518. <https://doi.org/10.1002/esp.2262>
- Mandlburger, G., Pfennigbauer, M., Pfeifer, N., 2013. Analyzing near water surface penetration in laser bathymetry - A case study at the River Pielach. *ISPRS Annals of Photogrammetry, Remote Sensing and Spatial Information Sciences II-5/W2*, 175–180. <https://doi.org/10.5194/isprsannals-II-5-W2-175-2013>
- McKean, J., Tonina, D., Bohn, C., Wright, C.W., 2014. Effects of bathymetric Lidar errors on flow properties predicted with a multi-dimensional hydraulic model: Lidar bathymetry and hydraulic models. *Journal of Geophysical Research: Earth Surface* 119, 644–664. <https://doi.org/10.1002/2013JF002897>
- Norris, C.W., Mounton, D.W., El-Hage, A., Bradsby, D., 2005. Ecologically Significant River and Stream Segments of Region L (South Central) Regional Water Planning Area (No. WRTS-2005-01), Sport Fish & Wildlife Restoration. Texas Parks and Wildlife Department, Austin, Texas.
- O'Dell, J.W., 1993. Method 180.1: Determination of turbidity by nephelometry (No. Revision 2.0). Office of Research and Development, U.S. Environmental Protection Agency, Cincinnati, OH.
- Paine, J.G., White, W.A., Smyth, R.C., Andrews, J.R., Gibeaut, J.C., 2005. Combining EM and Lidar to Map Coastal Wetlands: An Example from Mustang Island, Texas. *Environment and Engineering Geophysical Society*, pp. 745–756. <https://doi.org/10.4133/1.2923527>

- Paine, J.G., White, W.A., Smyth, R.C., Andrews, J.R., Gibeaut, J.C., 2004. Mapping Coastal Environments with Lidar and EM on Mustang Island, Texas, U.S. *The Leading Edge* 23, 894–898. <https://doi.org/10.1190/1.1803501>
- Pan, Z., Glennie, C., Hartzell, P., Fernandez-Diaz, J., Legleiter, C., Overstreet, B., 2015. Performance assessment of high resolution airborne full waveform Lidar for shallow river bathymetry. *Remote Sensing* 7, 5133–5159. <https://doi.org/10.3390/rs70505133>
- Preisendorfer, R.W., 1986. Secchi disk science: visual optics of natural waters: Secchi disk science. *Limnology and Oceanography* 31, 909–926. <https://doi.org/10.4319/lo.1986.31.5.0909>
- Saylam, K., 2016. A tale of two airborne Lidar scanners— lower Colorado River basin survey. *Lidar Magazine* 6, 34–37.
- Saylam, K., Hupp, J., Averett, A., Gutelius, B., Gelhar, B., 2018. Airborne Lidar bathymetry: Assessing quality assurance and quality control methods with Leica Chiroptera examples. *International Journal of Remote Sensing*. <https://doi.org/10.1080/01431161.2018.1430916>
- Saylam, K., Hupp, J.R., Aaron, R.A., 2017. Quantifying the bathymetry of the lower Colorado River basin, Arizona, with airborne Lidar. Presented at the IGTF ASPRS 2017 Annual Conference, researchgate, Baltimore, Maryland, pp. 1–11.
- Suk, N.S., Guo, Q., Psuty, N.P., 1998. Feasibility of using a turbidimeter to quantify suspended solids concentration in a tidal saltmarsh creek. *Estuarine, Coastal and Shelf Science* 46, 383–391. <https://doi.org/10.1006/ecss.1997.0284>

Appendix A

CORS horizontal and vertical accuracy reporting by NGS

Station: TXLE



Station: TXUV

